Electrochemistry Communications 24 (2012) 43–46

Contents lists available at SciVerse ScienceDirect

Electrochemistry Communications

journal homepage: www.elsevier.com/locate/elecom

Mg deposition observed by *in situ* electrochemical Mg K-edge X-ray absorption spectroscopy

Timothy S. Arthur [a,*], Per-Anders Glans [b], Masaki Matsui [a], Ruigang Zhang [a], Biwu Ma [c], Jinghua Guo [b]

[a] Toyota Research Institute of North America, 1555 Woodridge Ave, Ann Arbor, MI 48105, United States
[b] Advanced Light Source, Lawrence Berkeley National Laboratory, 1 Cyclotron Road, Berkeley, CA 94720, United States
[c] The Molecular Foundry, Lawrence Berkeley National Laboratory, 1 Cyclotron Road, Berkeley, CA 94720, United States

ARTICLE INFO

Article history:
Received 23 July 2012
Received in revised form 15 August 2012
Accepted 18 August 2012
Available online 24 August 2012

Keywords:
In situ electrochemical/XAS
Magnesium batteries
Interface analysis
Electrodeposition

ABSTRACT

The electrochemical deposition of magnesium from $[Mg_2(\mu\text{-}Cl)_3\cdot 6(OC_4H_8)]^+$ has been monitored *in situ* with X-ray absorption spectroscopy. The viability of the cell design was confirmed by a reversible shift in the X-ray absorption near-edge spectroscopy (XANES) of the Mg K-edge. *In situ* electrochemical XANES revealed the presence of an interfacial Mg intermediate below the equilibrium Mg/Mg^{2+} potential. A new method has been established to directly observe the complex electrochemical reduction process from Mg electrolytes.

1. Introduction

For long-range automotive transport, energy storage systems based on the multivalent Mg^{2+} ion are a promising alternative to lithium-ion batteries [1,2]. Magnesium metal (Mg) has a high volumetric capacity, 3833 mAh cm^{-3}, and dendrite-free deposition from organo-magnesium electrolytes [3–5]. However, methods to elucidate the mechanism for Mg deposition are pivotal for the design

lyte constituents with techniques such as *in situ* FT-IR, NMR, Raman and STM [6–11], however, high vacuum conditions ($<10^{-8}$ Torr) typically preclude the synchrotron analysis of air-sensitive, liquid systems. Cell development is crucial to harnessing the capabilities of powerful tools such as X-ray absorption spectroscopy (XAS) [12,13]. X-ray absorption near edge structure, XANES, is an element specific process that empirically determines the oxidation state of the absorbing species, which is ideal for looking at the deposition of Mg at a working electrode. Previously, Nakayama et al. used XAS to study the Mg and Al K-edge of magnesium organohaloaluminate and Grignard electrolytes [14]. The electrolytes used for this study, although fully functional for Mg deposition/dissolution, contain a mixture of RMgCl, R_2Mg, $MgCl_2$ (R = ethyl, butyl) and possible other Mg species. As a result, distinguishing the active species with XAS is a difficult task.

However, the crystallization of magnesium electrolytes from the mixture of a Lewis acid and a Lewis base isolates an active cation, $[Mg_2(\mu\text{-}Cl)_3\cdot 6(OC_4H_8)]^+$, for Mg deposition/dissolution [8,15]. Although unlikely, one possible route for the electro-reduction to form Mg is electron transfer to $[Mg_2(\mu\text{-}Cl)_3\cdot 6(OC_4H_8)]^+$ at the surface

AS measurements
ring the influence
e direct reduction

of the Mg-dimer, an *in situ* electrochemical XAS cell has been developed to directly study the interface of Mg deposition. Herein we report the Mg K-edge (~1300–1312 eV) XAS of $[Mg_2(\mu\text{-}Cl)_3\cdot 6(OC_4H_8)]^+$ during Mg deposition.

2. Material and methods

2.1. In situ cell design

Fig. 1a shows a cross-sectional drawing of the *in situ* electrochemical XAS cell, which builds upon previous liquid-compatible cells [13]. The material of interest was sealed with a Teflon O-ring (v) behind a 100 nm thick Si_3N_4 window (viii) etched into a 1 cm × 1 cm silicon wafer (vii). The Si_3N_4 window was sputtered with 40 nm of platinum on one side to serve as a working electrode (vi). The geometry of the cell is ideal to probe the electrochemical interface through the thin

* Corresponding author. Tel.: +1 734 995 0674; fax: +1 734 995 2549.
E-mail addresses: tim.arthur@tema.toyota.com (T.S. Arthur), paglans@lbl.gov (P.-A. Glans), masaki.matsui@tema.toyota.com (M. Matsui), ruigang.zhang@tema.toyota.com (R. Zhang), BWMa@lbl.gov (B. Ma), jguo@lbl.gov (J. Guo).

1388-2481
http://dx.doi.org/10.1016/j.elecom.2012.08.018

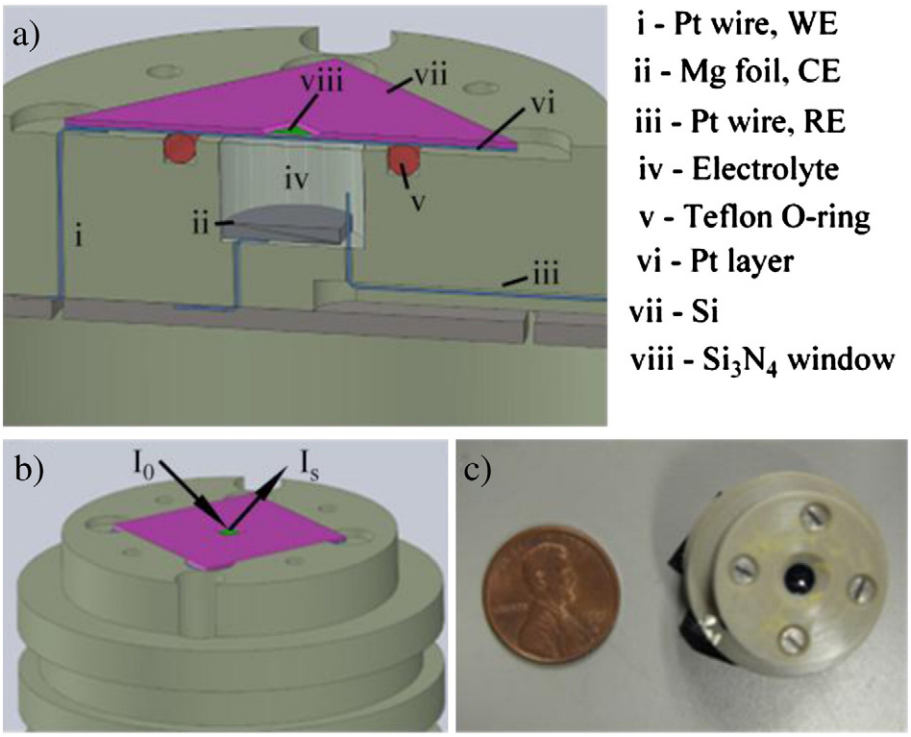

Fig. 1. a) Cross-section of the *in situ* electrochemical/XAS cell with annotations. b) Drawing and c) photograph of the assembled cell.

platinum layer (Fig. 1b). Two additional electrodes, Mg foil and a platinum wire (ii and iii), were inserted into the base of the cell.

2.2. Cyclic voltammetry

The open-circuit potential (OCP) of the three electrode cell was 0.06 V *vs* Mg RE. All cyclic voltammograms were scanned at 25 mV s^{-1} from OCP to −0.5 V *vs* Mg RE to 1.0 V *vs* Mg RE and finally back to the original OCP value. The surface area of the electrode was determined by the diameter of the electrolyte well (Fig. 1a, iv) and is 0.126 cm^2.

2.3. XAS data and analysis

The Mg K-edge was detected by fluorescence on beam-line 6.3.1 at the Advanced Light Source at Lawrence Berkeley National Lab. At the Mg absorption edge (45° incidence geometry), 100 nm Si_3N_4 window has a transmission of 94% of X-ray, 40 nm thick of Pt layer transmits 78%, which amounts to ~72% transmission for incoming X-ray to the liquid. Scattered X-rays from liquid travel through the same layers with ~72% transmission to the diode detector. All energies were calibrated with a MgO standard. The XAS data was processed with the Athena program from the HORAE software package [18].

2.4. Electrolyte synthesis and X-ray diffraction

In an Ar-filled glovebox (O_2 and H_2O<0.1 ppm), the white electrolyte powder was prepared by crystallizing 2:1 (Mg:Al) mixture of ethylmagnesium chloride and diethylaluminum chloride in tetrahydrofuran (THF) by solvent layering with hexanes. The white precipitate was washed with hexanes, dried under vacuum and re-dissolved in THF. The process was repeated thrice to yield white, needle-like crystals. This technique has been shown to yield electro-active crystals when re-dissolved in THF [8,15]. All chemicals are from Sigma Aldrich and used as received. Powder X-ray diffraction, XRD, was conducted on a Rigaku automated multipurpose X-ray diffractometer (Smartlab) equipped with Cu Kα radiation.

3. Results and discussion

3.1. Cell validation and Mg deposition

The magnesium salt used in this study was consistent with a $[Mg_2(\mu\text{-}Cl)_3 \cdot 6(OC_4H_8)](AlCl_4)$ solid crystals as seen by single crystal X-ray diffraction. Details to chemical analysis will be reported in a future manuscript, but the structure is similar to a reported active electrolyte [8]. The electrolyte consists of a 0.45 M solution of the crystals dissolved in THF. As shown in Fig. 2a, deposition and dissolution of magnesium were monitored through two- and three-electrode cyclic voltammograms between the sputtered Pt layer (Fig. 1vi, working) and the Mg foil (Fig. 1ii, counter). To generate the three-electrode cell, a Mg reference was galvanostatically deposited on to the Pt wire electrode (Fig. 1iii) using the Mg foil as a counter. The cycling efficiency, calculated from the charge balance, is greatly improved through the deposition of a Mg reference electrode onto the Pt wire, from 83% to 100%. For *in situ* XAS analysis, the deposition of the magnesium reference was performed without the two-electrode cyclic voltammograms to avoid a possible parasitic byproduct. In the three-electrode configuration, the deposition/dissolution maintained 100% cycling efficiency over 50 cycles. The start of Mg deposition, ($j = 1$ mA cm^{-2}), was determined to be −0.2 V *vs* Mg RE in the three-electrode configuration.

Fig. 2b shows the XANES evidence, normalized to the edge maximum, for the formation of Mg. After a galvanostatic reduction at $j = -15$ mA cm^{-2} for 3600 s, the edge energy shifted from 1311 eV to 1301 eV, the same value as Mg foil. Fig. 2c shows an X-ray diffraction pattern of the Si_3N_4 window confirming the deposition of Mg. The thickness of the Mg layer is coulometrically estimated to be 132 nm. An oxidation current of $j = +15$ mA cm^{-2} applied for 3600 s caused the edge to shift back to the original, as-prepared energy. Furthermore, the high efficiency of the process effectively removes Mg through

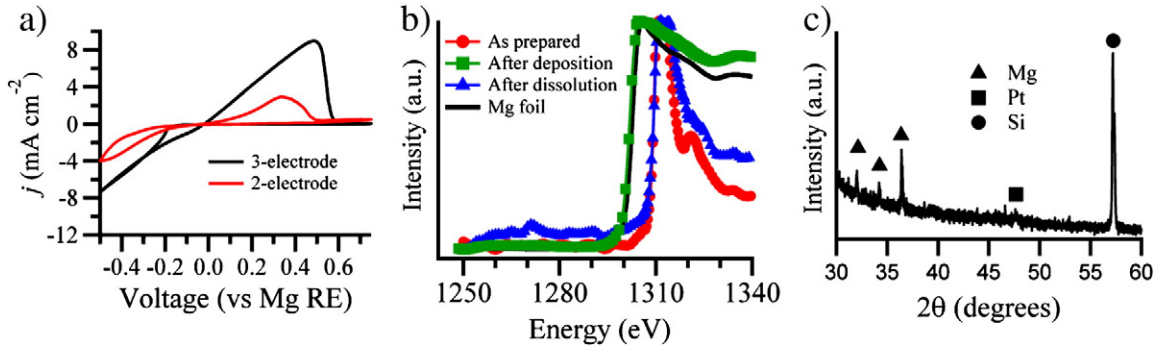

Fig. 2. a) CVs of the two- and three-electrode *in situ* electrochemical/XAS cell ($\nu = 0.025$ V s^{-1}). b) XANES region for the Mg K-edge of the as prepared cell and after galvanic Mg deposition/dissolution. Mg metal foil is shown as a reference. c) XRD pattern of the Si_3N_4 window after galvanic reduction at $j = -15$ mA cm^{-2} for 3600 s.

an equivalent anodic charge with minimal decomposition of the electrolyte.

3.2. In situ potentiostatic X-ray absorption measurements

In situ potentiostatic X-ray absorption (PSXA) experiments were designed to gain deeper insights to the interface between the electrode and the electrolyte during deposition. Fig. 3a shows the three potentials, −0.1 V, −0.2 V and −0.4 V *vs* Mg RE, chosen from the cathodic wave for the PSXA experiments. The potential V = −0.2 V is the start of Mg deposition, and −0.1 V and −0.4 V represent potentials before and after Mg deposition, respectively. Fig. 3b shows the XANES region for the PSXA spectra. The growth of a low-energy edge is evidence of an additional magnesium absorber at the interface of the platinum and the electrolyte. By applying lower potentials, the size of the wave increases and the edge energy decreases toward the position for Mg. A potentiostatic deposition at V = −0.1 V *vs* Mg RE for t = 10,800 s did not show a diffraction pattern for crystalline Mg or an XAS signature for Mg metal. The presence of a XANES signal V = −0.1 *vs* Mg RE is an interesting result because the additional edge is observed before V = −0.2 V *vs* Mg RE, the start of Mg deposition. The XANES results indicate that the presence of a Mg species besides the Mg-dimer is required before the deposition of Mg.

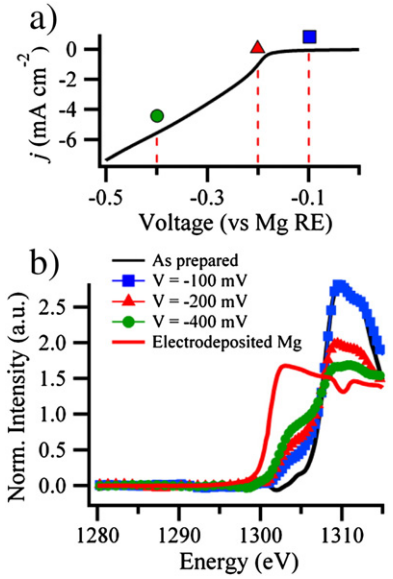

Fig. 3. a) Cathodic wave for the deposition of Mg from a 0.45 M electrolyte solution with marked potentials for the PSXA experiments. b) XANES region of the Mg K-edge marked in a).

The exact stoichiometry and structure of the species at interface of Mg deposition remains unknown, but we can infer additional structural information from future extended X-ray absorption fine structure analysis. Previously, energy-induced intermediates have previously been seen with XANES. For example, Martin-Diaconescu and Kennepohl have observed the growth of pre-edge features attributed to radical species for photochemically oxidized glutathione at the sulfur K-edge [19]. Considering the current XAS data and analysis that compliment previous studies [3,10], a direct electrochemical reduction of the Mg-dimer is an unlikely route to form Mg.

4. Conclusion

A UHV-compatible electrochemical/XAS cell has been developed to study the complex electrochemical Mg reduction process. *In situ* potentiostatic X-ray absorption spectroscopy of the Mg K-edge was used to study the electrode/electrolyte interfacial species, in which XANES analysis revealed the presence of an intermediate species at potentials below the deposition potential for Mg. As a next step, we will study the *in situ* dissolution of Mg which is the other vital process to further understand the electrochemical mechanisms at the Mg battery anode. Through *in situ* electrochemical XAS techniques, we have gained valuable insights toward the development of next generation Mg electrolytes.

Acknowledgments

The work at ALS and The Molecular Foundary is supported by the U.S. Department of Energy under the contract no. DE-AC02-05CH11231.

References

[1] D. Aurbach, Z. Lu, A. Schechter, Y. Gofer, H. Gizbar, R. Turgeman, Y. Cohen, M. Moshkovich, E. Levi, Nature 407 (2000) 724.
[2] J.M. Tarascon, M. Armand, Nature 414 (2001) 359.
[3] D. Aurbach, I. Weissman, Y. Gofer, E. Levi, Chemical Record 3 (2003) 61.
[4] M. Matsui, Journal of Power Sources 196 (2011) 7048.
[5] T.D. Gregory, R.J. Hoffman, R.C. Winterton, Journal of the Electrochemical Society 137 (1990) 775.
[6] D. Aurbach, Y. Cohen, M. Moshkovich, Electrochemical and Solid-State Letters 4 (2001) A113.
[7] D. Aurbach, G.S. Suresh, E. Levi, A. Mitelman, O. Mizrahi, O. Chusid, M. Brunelli, Advanced Materials 19 (2007) 4260.
[8] H.S. Kim, T.S. Arthur, G.D. Allred, J. Zajicek, J.G. Newman, A.E. Rodnyansky, A.G. Oliver, W.C. Boggess, J. Muldoon, Nature Communications 2 (2011) 427.
[9] Y. Vestfried, O. Chusid, Y. Goffer, P. Aped, D. Aurbach, Organometallics 26 (2007) 3130.
[10] D. Aurbach, R. Turgeman, O. Chusid, Y. Gofer, Electrochemistry Communications 3 (2001) 252.
[11] N. Pour, Y. Gofer, D.T. Major, D. Aurbach, Journal of the American Chemical Society 133 (2011) 6270.

[12] P. Jiang, J.-L. Chen, F. Borondics, P.-A. Glans, M.W. West, C.-L. Chang, M. Salmeron, J. Guo, Electrochemistry Communications 12 (2010) 820.
[13] J.H. Guo, A. Augustsson, S. Kashtanov, D. Spangberg, J. Nordgren, K. Hermansson, Y. Luo, Journal of Electron Spectroscopy and Related Phenomena 144–147 (2005) 287.
[14] Y. Nakayama, Y. Kudo, H. Oki, K. Yamamoto, Y. Kitajima, K. Noda, Journal of the Electrochemical Society 155 (2008) A754.
[15] J. Muldoon, C.B. Bucur, A.G. Oliver, T. Sugimoto, M. Matsui, H.S. Kim, G.D. Allred, J. Zajicek, Y. Kotani, Energy & Environmental Science 5 (2012) 5941.
[16] E.M. Erickson, M.S. Thorum, R. Vasic, N.S. Marinkovic, A.I. Frenkel, A.A. Gewirth, R.G. Nuzzo, Journal of the American Chemical Society 134 (2012) 197.
[17] F. Zheng, S. Alayoglu, J. Guo, V. Pushkarev, Y. Li, P.-A. Glans, J.-l. Chen, G. Somorjai, Nano Letters 11 (2011) 847.
[18] B. Ravel, M. Newville, Journal of Synchrotron Radiation 12 (2005) 537.
[19] V. Martin-Diaconescu, P. Kennepohl, Journal of the American Chemical Society 129 (2007) 3034.